Surface & Coatings Technology 204 (2010) 3887–3894

Contents lists available at ScienceDirect

Surface & Coatings Technology

journal homepage: www.elsevier.com/locate/surfcoat

Effect of nitrogen ion irradiation on the nano-tribological and surface mechanical properties of ultra-high molecular weight polyethylene

Laura Fasce [a,*], Josefina Cura [a], Mariela del Grosso [b,c], Gerardo García Bermúdez [b,c,d], Patricia Frontini [a]

[a] Instituto de Investigaciones en Ciencia y Tecnología de Materiales (INTEMA), Universidad Nacional de Mar del Plata – CONICET, Argentina
[b] Gerencia de Investigación y Aplicaciones, Tandar, Comisión Nacional de Energía Atómica, Argentina
[c] Concejo Nacional de Investigaciones Científicas y Técnicas, (CONICET), Argentina
[d] Escuela de Ciencia y Tecnología, Universidad Nacional de San Martín (UNSAM), Argentina

ARTICLE INFO

Article history:
Received 17 December 2009
Accepted in revised form 6 May 2010
Available online 1 June 2010

Keywords:
Polyethylene
Nano-indentation
Elastic properties
Nano-wear

ABSTRACT

Generation of wear debris is the principal obstacle limiting the durability of ultra-high molecular weight polyethylene (UHMWPE) in biomedical applications. Aiming to enhance UHMWPE wear resistance, surface modification with swift heavy ion irradiation (SHI) appears as a potential and attractive methodology. Contrary to ion implantation techniques, the swift heavy ions range can reach tens to hundreds microns and its extremely high linear energy is able to induce effective chemical modifications using low fluence values. Nano-wear performance and surface mechanical properties of samples of pristine and SHI irradiated (using N_2^+ ions at 33 MeV and a fluence of 1×10^{12} ions/cm^2) were characterized by depth sensing indentation (DSI) and scanning probe microscopy (SPM). It turned out that modifications induced by irradiation at the surface layers were successful to reduce nano-wear volume and creep deformation. These improvements were related to beneficial changes in hardness, elastic modulus, hardness to elastic modulus ratio and friction coefficient.

1. Introduction

Ultra-high molecular weight polyethylene (UHMWPE) is the principal polymeric biomaterial used to replace damaged cartilage in joint implants due to its relatively high abrasion resistance [1]. However, articulation between metallic and UHMWPE components remains the standard of care in biomedical implant applications even today. Wear at the articulating surfaces occurs under normal usage conditions and it is a consequence of sliding movements between the metallic part and the polymeric counterpart. The generation of sub micron UHMWPE wear debris is recognized as one of the major causes of premature failure of the total joint replacement [2,3]. UHMWPE wear mechanism in joint implants is predominantly abrasive, but also other wear modes such as adhesive and delamination fatigue are present [4,5].

The most widespread way of improving UHMWPE wear resistance is by crosslinking of adjacent molecular chains using gamma (γ) or electron (*e*) beam irradiations [6]. It is believed that crosslinking prevents alignment of crystalline regions of UHMWPE (lamellae) parallel to the sliding direction, enhances the surface resistance to plastic shearing, thereby reducing wear debris formation [7,8]. In γ or *e* beam irradiation techniques, the energy deposition occurs homogenously over the whole volume of the sample [9]. The main disadvantage of these techniques is that wear improvement is accompanied by a decrease in bulk mechanical properties such as ultimate tensile strength, ductility, toughness and fatigue resistance [10]. Detriment in UHMWPE mechanical properties may have serious implications for devices exposed at high stress concentrations or large cyclic contact stresses, as in the case of total knee joint replacements.

The ideal solution to improve UHMWPE wear resistance without detriment of its bulk properties is to limit the modification to the surface layer of the material. Recent literature reports many data about the wear improvement of UHMWPE by using ion bombardment treatments such as ion implantation [11–16] and plasma immersion ion implantation [17–20]. The modified layer, which depends on the ion type and fluence (ions/cm^2), reaches depth values ranging from a few nanometers to one micrometer [12,16,21,22]. Swift heavy ion beams (SHI) irradiation is an alternatively good candidate for surface modification of UHMWPE [23–25]. Contrary to ion implantation techniques, the swift heavy ions range can reach tens to hundreds microns in UHMWPE and its extremely high linear energy is able to induce effective chemical modifications using lower fluence values. On their way through matter, SHI lose their energy to the electrons of the target leading to a continuous trail of excited and ionized target atoms along the ion path. The ejected electrons have a broad spectrum of kinetic energies and trigger a considerable number of further ionizations. Most of the primary processes occur close to the ion-trajectory in a cylindrical zone with a radius of a few nanometers, called “track core”. The energy deposited into such a small volume is extremely high and can reach

* Corresponding author. Universidad Nacional de Mar del Plata - CONICET Instituto de Investigaciones en Ciencia y Tecnología de Materiales (INTEMA) J. B. Justo 4302 Mar del Plata Argentina.
E-mail address: laura.fasce@gmail.com (L. Fasce).

0257-8972/$ – see front matter © 2010 Elsevier B.V. All rights reserved.
doi:10.1016/j.surfcoat.2010.05.005

several keV/nm^3. Processes induced by the cascade of the secondary electrons are spread over a much larger radial distance from the track core. The maximum range depends on the projectile velocity and may reach up to a micrometer perpendicular to the ion trajectory. Target ionization causes chemical transformations in the polymer such as chain scission, intermolecular crosslinking, double and triple bonds formation, creation of carbonaceous clusters and eventually ejection of hydrogen atoms [26–30].

M. del Grosso et al. showed that SHI irradiation can enhance the wear resistance of UHMWPE and that the wear improvement level depends on the ion type and fluence [23,24]. In a particular study, they irradiated a commercial grade UHMWPE at 33 MeV using N_2^+ ions and fluence values ranging from 5×10^{10} to 5×10^{14} ions/cm^2 and performed ball-on-disk wear tests [24]. The sample irradiated with a fluence of 1×10^{12} ions/cm^2 exhibited the better wear performance, showing a reduction in volume loss of about 40%. Encouraged by these results, nano-tribological behavior as well as surface mechanical properties of commercial UHMWPE and SHI irradiated UHMWPE were characterized in the present work.

Nano-tribological characterization is crucial to analyze the effect of SHI on UHMWPE because local wear and surface damage play a dominant role in the failure process of joint implants [31]. Wear damage at the nano-level (where the applied loads are very low) may be different to the forms of wear damage at large scale. This is because different primary deformation processes, low wear rates and presence of inertial forces are expected in low load wear conditions. Scanning Probe Microscopy (SPM) techniques such as nano-wear are sensitive enough to perform such characterization [32]. It is also of great concern to understand the effect of SHI on the surface mechanical properties that govern the main aspects of material's contact performance as well as to assess the mechanical behavior of UHMWPE on the scale at which wear particles generate during normal wear. Depth Sensing Indentation (DSI) techniques provide a wealth of valuable quantitative information regarding the surface mechanical behavior. They have been widely applied to characterize metals, ceramics, thin films and more recently polymeric materials including UHMWPE [12,13,15,33–38].

The aim of this investigation was to analyze the effect of a specific type of SHI irradiation that uses N_2^+ ions, energy of 33 MeV and fluence of 1×10^{12} ions/cm^2 on relevant UHMWPE properties. SPM and DSI techniques including nano-wear, nano-scratching, and nano and micro-indentations were applied to determine accurate values of nano-wear volume loss, elastic modulus, hardness, friction coefficient and creep parameters of both pristine and SHI irradiated UHMWPE.

2. Experimental

2.1. Materials

The pristine material used in this investigation was a medical grade UHMWPE (GUR 1050, Poly Hi Solidur). Cubic samples whose edge measured 1 cm were machined from the received block. For each sample, one of the six faces was polished using silicon carbide papers of progressively fine grade with water lubrication and finally with 1, 0.3 and 0.05 μm alumina particle size aqueous suspensions.

The polished face of the samples were irradiated with nitrogen (33 MeV) provided by the Buenos Aires Tandem Accelerator Tandar (20 MV) with a fluence of 1×10^{12} ions/cm^2 (hereafter N_2^+ UHMWPE sample). The samples were placed in a mechanical device that rotates in front of the beam. The actual ion fluence was determined by collecting ion current with a Faraday Cup during short times when the samples are out of the beam. According to calculations made by means of the Stopping and Range of Ions in Matter software (SRIM©-2006), the projected ion range for N_2^+ (33 MeV) reaches 40 μm [39].

Both type of samples (polished UHMWPE and N_2^+ irradiated UHMWPE) were kept in vacuum and darkness after being prepared. Nano-tribological as well as nano-mechanical tests were carried out under nitrogen atmosphere.

2.2. FTIR-ATR experiments

Studies regarding chemical changes induced by SHI irradiation on UHMWPE have been previously published [23–25]. In this work, complementary FTIR spectra were obtained using the attenuated total reflectance technique (ATR) in order to obtain information about chemistry and microstructure at the surface layers of the samples under research. Samples were kept in vacuum and darkness previous to FTIR testing. Spectra were recorded in a Nicolet 6700 (Thermo Scientific) FTIR spectrometer equipped with the Smart Orbit accessory with 64 scans using 4 cm^{-1} resolution.

2.3. Nano-wear experiments and depth sensing indentation tests

Surface roughness determinations, nano-wear experiments and depth sensing indentation tests were carried out at room temperature using a Triboindenter Hysitron equipped with Multi Range nanoprobe device (MRNP) and Scanning Probe Microscope module (SPM).

SPM images of the samples surfaces were obtained using a spherical tip (60° cone angle, 1 μm radius of curvature), a scan rate of 0.5 Hz and a set-point force of 2 μN. The arithmetic mean surface roughness (R_a) was calculated as the average of the absolute values of the surface height deviations measured from the mean plane within a box of 900 μm^2 in three different locations of each sample.

Nano-wear tests were carried out using a spherical tip of 60° cone angle and 1 μm radius of curvature as the hard asperity sliding against sample surface. Exploratory nano-wear experiments were performed in order to establish unique experimental conditions that cause wear damage in both types of samples. A normal force of 50 μN was applied while the tip moved 10 times at a frequency of 3 Hz over an area of 5×5 μm^2 on the sample surface. After the nano-wear process, topographic images of the worn area were obtained using a low force of 2 μN and a scanning frequency of 1 Hz. The amount of material removed from the surface, the so-called nano-wear volume, V, was determined by the analysis of the surface profiles across the worn area obtained from the SPM images [40]. V was defined as the difference between the grooved volume, V^-, and the pileups volume, V^+ (Fig. 1-*a*). The reported nano-wear volumes are the average of 5 replicated tests performed in each sample.

Indentation tests were performed using a diamond made Berkovich tip under load control conditions. Trapezoidal loading functions with maximum loads ranging from 1 mN to 1.3 N were applied. For each load condition, at least 10 indentations in different locations of the samples were made. The lowest load level was selected to keep surface roughness values (Ra) values lower than 10% of indentation depths. Thanks to the combination of nano-indentation (loads up to 10 mN) and micro-indentation devices (loads up to 2.2 N), depths from 1 up to 40 μm were achieved during experiments, being the largest value equal to the estimated length of the projected ion range. A holding period of 20 s was applied at maximum load between loading and unloading stages. Tip displacement was corrected by thermal drift as follows: Before the indentation test is started, the system leaves the tip on the sample and monitors any displacement of it; then, a “drift rate” is calculated as the slope of the displacement vs. time data, which is assumed to remain constant throughout the indentation test. In order to keep the total time of the loading/holding/unloading cycles lower than one minute, loading/unloading rates were set as 450 μN/s, 20 mN/s and 100 mN/s for indentations performed up to 10 mN, 200 mN and 1.3 N of maximum applied load, respectively.

Creep experiments involved indentations under load controlled conditions with application of a step load function: After a fast loading stage at 500 μN/s to limit relaxation phenomena, the load was held constant at 1000 μN during 56 s. During this period the tip

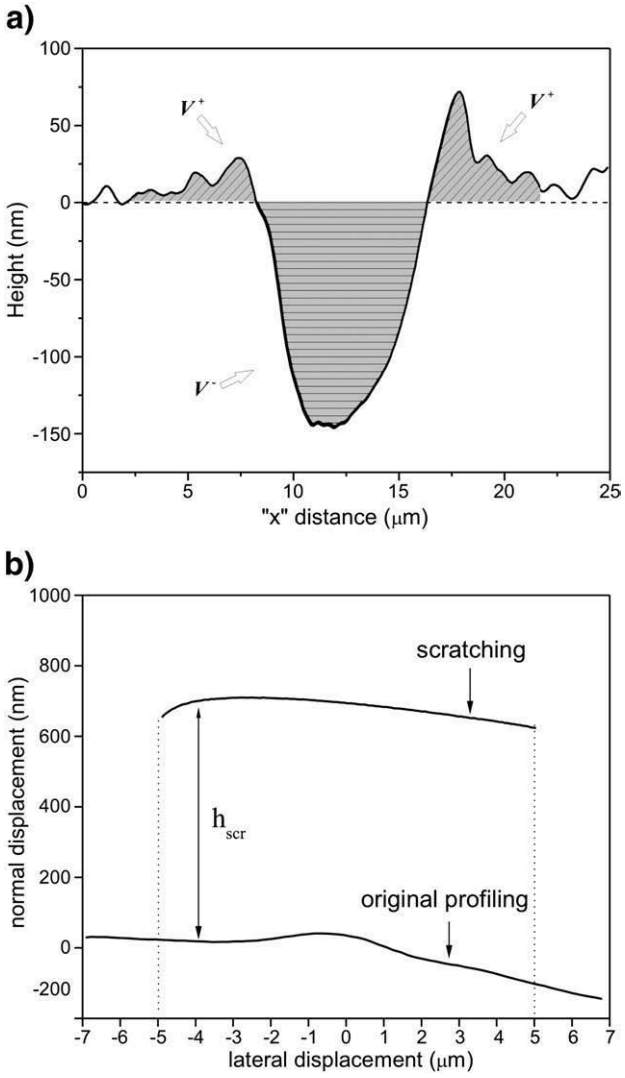

Fig. 1. Example of profile analysis used to determine: a) Nano-wear volume, V, from SPM images and b) Scratch depth, h_{scr}, in nano-scratch experiments.

displacement into the sample was recorded. For each sample, 16 creep experiments were performed.

Nano-scratch experiments were performed using a spherical tip with 20 μm radius of curvature. A single test involved three stages: original profiling, actual scratching with a sliding speed of 1 μm/s under a constant load of 3000 μN and final profiling. For each sample, ten nano-scratch experiments were carried out. The apparent friction coefficient (μ_{app}) was calculated according to the Amontons and Coulomb law, as the ratio of the measured tangential (F_x) and normal (F_z) forces during the nanoscratching stage. In addition, the scratch penetration depth (h_{scr}) was calculated using the original profile as reference (Fig. 1-*b*).

2.4. Data reduction

The analysis for the tip area calibration and the calculation of reduced elastic modulus (E_r) and universal hardness (H) were conducted using the approach outlined by Oliver and Pharr [41]. This method is based on the assumption that the material behavior during unloading is purely elastic. According to O&P proposal, the unloading part of the recorded load–depth (P–h) curve was fitted through a power law function:

$$P = A(h - h_f)^m \tag{1}$$

and the contact stiffness (S) was calculated from slope of unloading curve as:

$$S = \left.\frac{dP}{dh}\right|_{h_{max}} = mA(h_{max} - h_f)^{m-1} \tag{2}$$

where A and m are the power law function fitting parameters, h_f is the residual penetration depth and h_{max} was taken as the maximum penetration depth achieved after the holding period.

The contact depth h_c was calculated by:

$$h_c = h_{max} - \varepsilon\frac{P_{max}}{S} \tag{3}$$

being ε a tip geometry factor, usually taken as 0.75.

Reduced elastic modulus (E_r) and hardness (H) were then calculated as:

$$E_r = \frac{S\sqrt{\pi}}{2\sqrt{A_c}} \tag{4}$$

$$H = \frac{P\,max}{A_c} \tag{5}$$

where A_c is the actual contact area which accounts for the non-ideal shape of the tip. For indentation depths lower than 6 μm, A_c was fitted to a polynomial function of h_c using a series of indentations performed on a polycarbonate standard. For indentation depths larger than 6 μm, A_c was assumed to be the ideal Berkovich ($A_c = 24.5h_c^2$).

E_r is directly related to the Young modulus of the material by:

$$E_r = \left[\frac{1-\nu^2}{E} + \frac{1-\nu_i^2}{E_i}\right]^{-1} \tag{6}$$

being E_i and ν_i are the Young modulus and the Poisson´s ratio of the indenter (1140 GPa and 0.07) while E and ν are the sample properties.

The initial phase of creep was fitted to a simple phenomenological approach, which has been shown to be suitable to describe the rate and extent of the time-dependent deformation of UHMWPE among several polymers [42]. In this approach, the recorded indentation depth during dwell, h, is described by two parameters as follows:

$$\frac{h}{h(0)} = \frac{A}{h(0)}\ln(B\cdot t + 1) \tag{7}$$

where $h(0)$ is the maximum penetration depth reached under loading, $A/h(0)$ is a dimensionless term which accounts by the creep extent and allows material comparison and B is a rate term.

2.5. SEM analysis

Scanning electron microscopy (SEM) micrographs were obtained using a JEOL JSM-6460LV scanning electron microscope operating at an accelerated voltage of 15 kV. After testing, UHMWPE and N_2^+UHMWPE sample surfaces were coated with a thin layer of gold.

3. Results and discussion

3.1. Nano-wear volume

SEM inspection and SPM analysis revealed that N_2^+ irradiation did not induce modifications of the surface roughness of UHMWPE. Polished UHMWPE sample as well as polished and N_2^+ irradiated UHMWPE sample exhibited surface roughness values (Ra) ranging from 70 to 100 nm.

SPM images of UHMWPE and N_2^+UHMWPE samples surfaces containing one of the worn areas are shown in Fig. 2. It appears that under the same load and sliding conditions, the damage displayed in N_2^+UHMWPE sample was considerably lower than the one developed

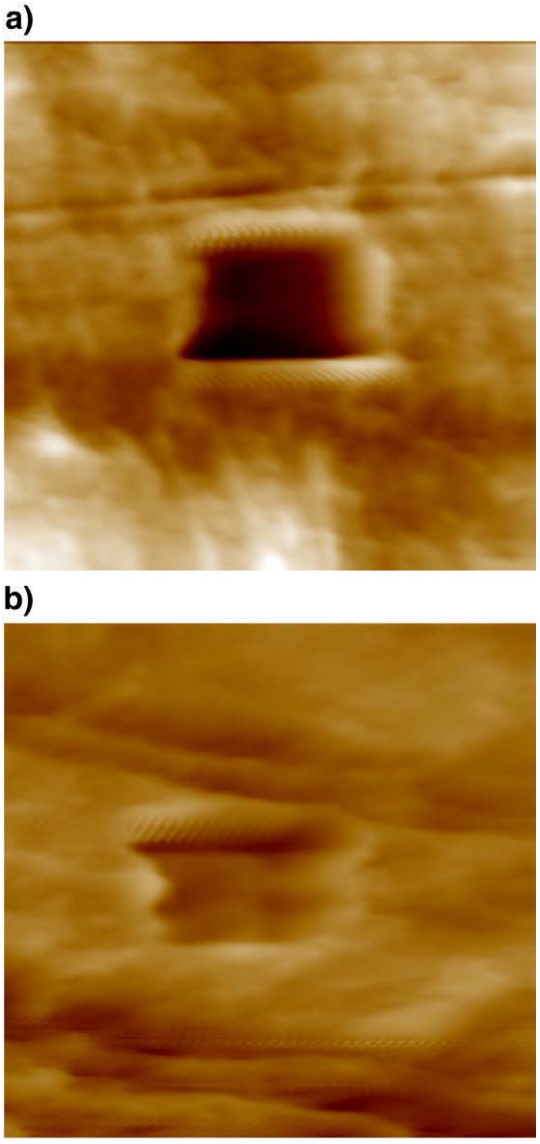

Fig. 2. Typical SPM images obtained after nano-wear experiments in a) UHMWPE and b) N_2^+UHMWPE surfaces. Images scan size is 25×25 μm.

in UHMWPE. For both polymers, well-defined pileups on the edges of the worn area appeared. These pileups resemble the ones observed in UHMWPE nano-scratch experiments by Ping Wong et al. [32]. According to the height profile analysis, the material volume forming the pileups was lesser than the material volume lacking from the worn area. SEM micrograph of Fig. 3 revealed that pileups were formed as a consequence of material movement by plastic deformation and that polymer molecules were actually removed from the surface by a cutting or delamination mechanism [43].

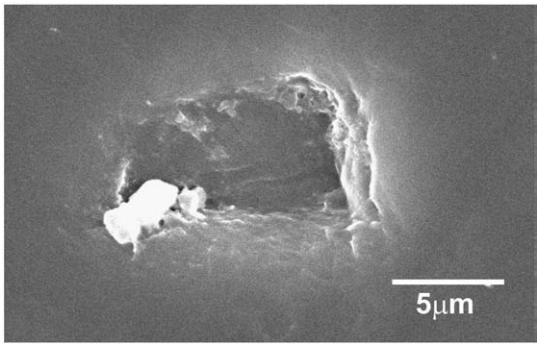

Fig. 3. SEM image showing one of the worn areas developed in N_2^+UHMWPE sample after nano-wear test.

Average nano-wear volume values are reported in Table 1 for both materials. It emerges that N_2^+ irradiation promoted a striking reduction in material loss of about 90%. Moreover, during exploratory experiments, there were several conditions at which no material loss was observed in N_2^+UHMWPE while it was appreciable in UHMWPE.

It appeared that N_2^+ irradiation retarded the cutting or delamination process that leads to the generation of wear particles in UHMWPE. So that, nano-wear behavior of UHMWPE was significantly improved by N_2^+ irradiation.

3.2. Elastic modulus and hardness

Load–depth indentation curves of UHMWPE and N_2^+UHMWPE samples are shown in Fig. 4. Both materials displayed load hysteresis indicative of irreversible deformation and showed creep during the holding period. Accordingly, a permanent indent was left on the samples surface after indentation (Fig. 5). The different shape of indentation curves of both samples indicates that irradiation changed the mechanical response of the surface layers of UHMWPE.

Indentation curves were first analyzed in terms of the Oliver and Pharr approach (O&P) [41] as described in Section 2.4 because this is the simplest and most widespread method in depth sensing indentation to determine material's elastic modulus and hardness [44,45]. But, Eq. (1) did not give a good fit to the onset portion of the unload curves due to viscoelastic response of the polymers (indentation creep effects). The hold times and unloading rates that could be practically achieved were not high enough to minimize creep effects in the studied polymers [36,46,47]. So, in order to obtain reliable properties, a simple post-experiment data procedure proposed by Ngan et al. [47–49] was applied. A corrected elastic stiffness, S_e, was determined from:

$$\frac{1}{S_e} = \frac{1}{S_u} + \frac{\dot{h}}{\dot{P}_u} \tag{8}$$

where S_u is the apparent contact stiffness at the onset of unloading, $\dot{h}$ is the tip displacement rate at the end of the load hold just prior to unloading and $\dot{P}_u$ is the unloading rate. The calculated S_e value replaced S in Eqs. (3) and (4) for E_r and H calculations.

E_r and H values as a function of maximum penetration depth (h_{max}) are plotted in Fig. 6. Several observations can be drawn:

- A gap in elastic modulus values determined from nano and micro-indentations is observed for both samples due to the great difference in deformation rate imposed in each type of test (Section 2.3). As expected, increasing the deformation rate resulted in an increase in the elastic modulus values.
- An increasing trend of hardness with increasing indentation depth is observed at low penetration depths (in nano-indentations range) (Fig. 6b). This trend has been already observed in UHMWPE nanoindentation studies and attributed to the lesser constrained molecular movement at the near surface than at the bulk state [31].
- A wide scattering in E_r and H values is observed at indentation depths lower than 5 μm. The scattering is notably reduced at larger indentation depths. Scattering has been previously observed in nano-mechanical properties of UHMWPE [15,38]. Scattering in nano-indentations may arise from inadequate surface roughness which influences the tip contact. However, surface roughness effects were found to shift the average values of the evaluated properties [50]. Other possible source of scattering is the local variation of material behavior itself. At low depths, the dimensions of the sharp Berkovich indenter is closed to the size of the amorphous layers and crystalline lamellae domains of UHMWPE

Table 1
Summary of properties determined from SPM and DSI experiments.

Test	Nano-wear	Indentation	Creep		Scratch	
	V (μm^3)	H/E_r	A/h_0	B	μ_{app}	h_{scr} (nm)
UHMWPE	2.70	0.038	0.052 ± 0.002	1.64 ± 0.08	0.232 ± 0.006	943 ± 47
N_2^+UHMWPE	0.17	0.041	0.0025 ± 0.002	7.27 ± 1.24	0.161 ± 0.011	737 ± 9

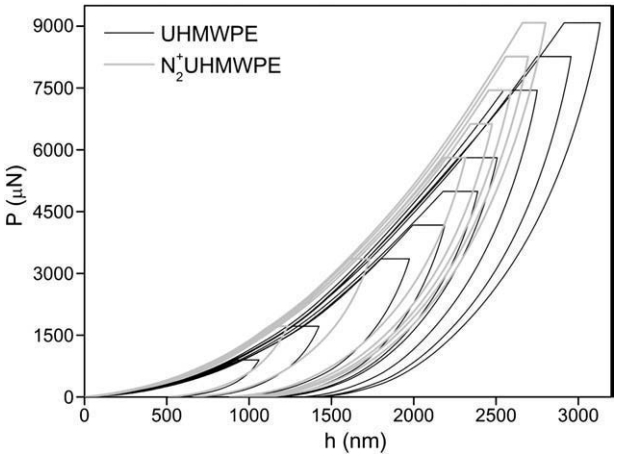

Fig. 4. Typical load–penetration depth curves obtained in depth sensing indentation experiments.

(see for example TEM images of GUR1050 published elsewhere [31]). As these two components exhibit different contact deformation properties, it is expected that local mechanical response from one point to another on the surface differs. At high loads, the large volume involved under the indenter mediates the contributions of both phases, so that indentation response turns out to be homogeneous.

- N_2^+UHMWPE showed higher elastic modulus and hardness values than UHMWPE in the whole penetration depth length achieved in the experiments. Hardness was slightly more affected than stiffness by N_2^+ ion irradiation, so that the H/E_r ratio of the modified layer was larger than the one of the pristine polymer. H/E_r values at a depth of 5 μm are listed in Table 1 for comparison.
- N_2^+UHMWPE behaved as a stiffed surface graded material since it displayed a decreasing trend in reduced elastic modulus and hardness with increasing penetration depth (refer only the micro-indentation range data in Fig. 6). Fissher-Cripps demonstrated through finite element analysis that for the case of a stiff surface graded material, O&P elastic modulus and hardness could underestimate the actual properties of the material [51].

Summarizing, it can be assure that the used N_2^+ irradiation led to a near surface layer with enhanced hardness, elastic modulus and hardness to elastic modulus ratio. Taking into account that hardness is directly proportional to yield stress [52,53], N_2^+ irradiation induced a beneficial increase of UHMWPE resistance to plastic deformation at the near surface layers. For polymers, the increase in hardness contributes to the improvement of abrasive wear resistance [54,55]. On the other hand, the larger H/E_r ratio limits the plastic deformation while extends the elastic deformation of the surface layer. Thus, the adhesive wear resistance of UHMWPE is improved [21].

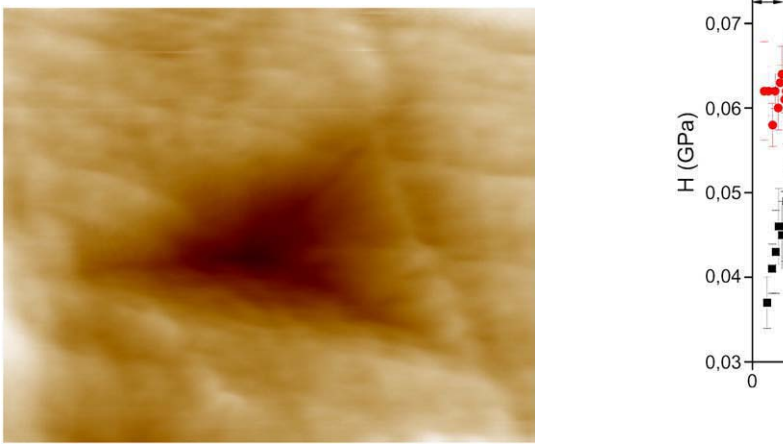

Fig. 5. SPM image of UHMWPE surface after indentation with a Berkovich tip at 1 mN of maximum applied load.

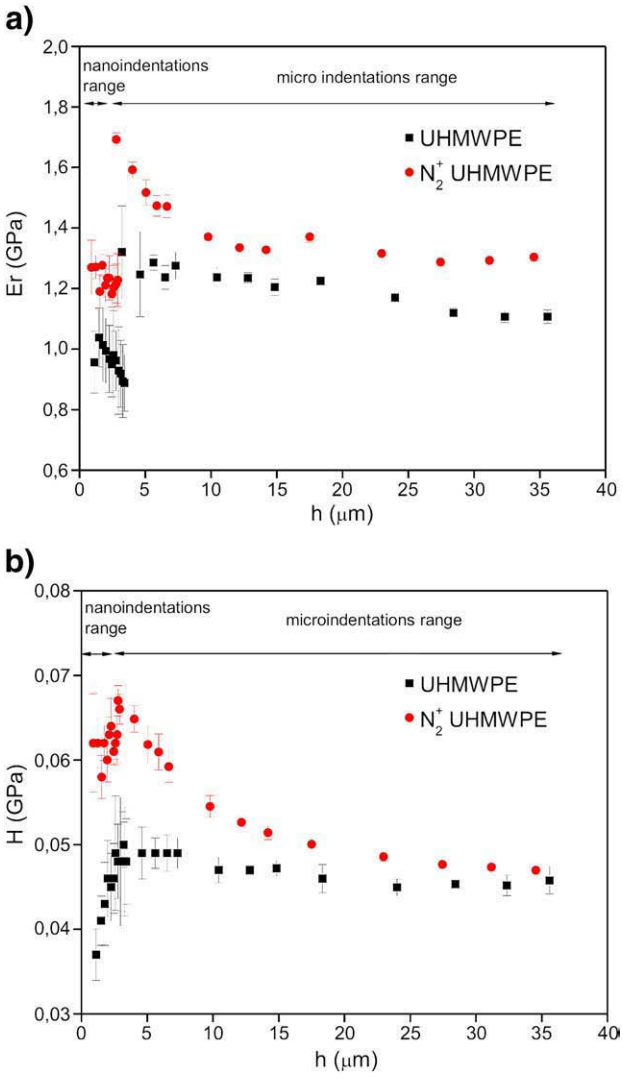

Fig. 6. Comparison of surface mechanical properties *vs.* indentation depth obtained from depth sensing indentation experiments in UHMWPE and N_2^+UHMWPE samples: a) Reduced elastic modulus and b) Hardness.

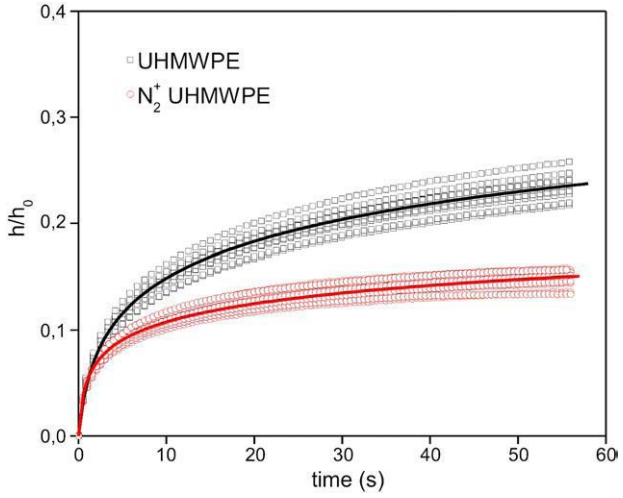

Fig. 7. Fractional increase in depth during creep experiments for UHMWPE and N_2^+UHMWPE samples. Filled curves were constructed considering the average fitted parameters of Eq. (7).

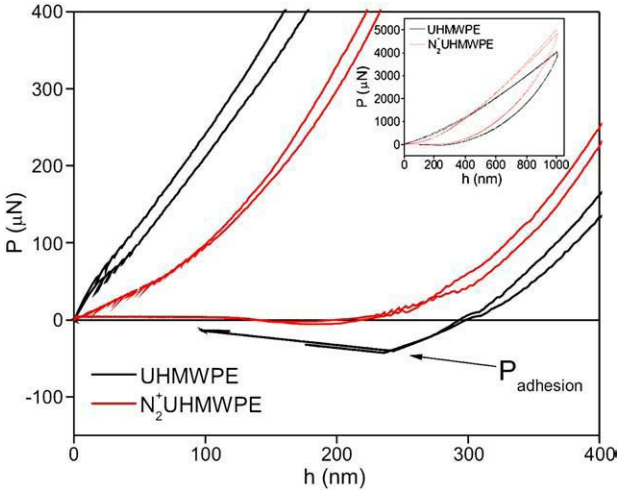

Fig. 9. Load–penetration depth curves obtained in indentation experiments using a 20 μm-tip-radius spherical indenter under displacement controlled conditions.

3.3. Creep

In order to evaluate the effect of N_2^+ irradiation on the time dependent properties of UHMWPE indentation creep experiments were carried out. Fig. 7 shows the increase in depth of the Berkovich indenter after the application of a step load as a function of dwell time. The fitted $A/h(0)$ and τ parameters are listed in Table 1.

N_2^+ irradiation changed the pronounced time dependent mechanical response of UHMWPE. The creep extent ($A/h(0)$) was reduced by ~50% and the creep rate (B) increased about 4.5 times. These results are consistent with the increase in elastic modulus and yield stress of the surface layers observed after N_2^+ irradiation. According to Eyring theory, for a creep event to occur the polymer chains must overcome a potential barrier by thermal activation. Application of a stress has the effect of reducing the potential barrier and increasing the rate at which jumps occur. So that, the creep rate was faster in the N_2^+ UHMWPE sample because it has high values of elastic modulus and yield stress and hence the stress field developed under the indenter was higher.

3.4. Friction coefficient

Fig. 8 shows the tangential to normal force ratio measured during scratch experiments as a function of the sliding displacement for UHMWPE and N_2^+UHMWPE samples. As expected, little effect of surface roughness is observed in the measurements because the tip radius of the spherical indenter was large in comparison with surface roughness. The measured force ratio stabilized at a scratch distance of about 0.5 μm approaching a constant value, which was taken as the apparent friction coefficient. The determination of this parameter was not influenced by the presence of removed particles since SEM examination performed after testing revealed complete deformation recovery of the scratch grooves.

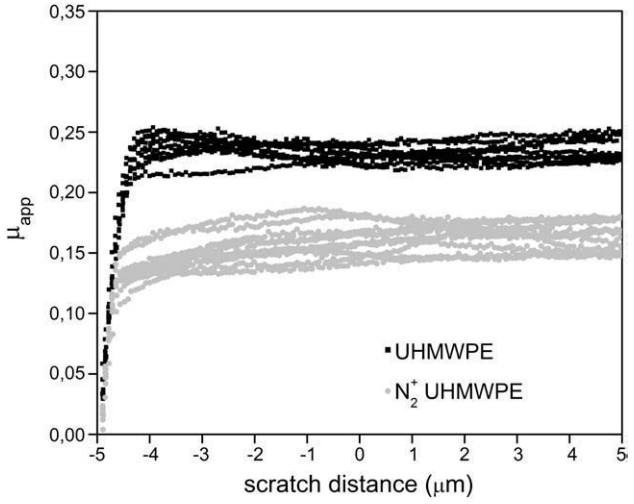

Fig. 8. Apparent friction coefficient *vs.* scratch distance plots obtained in nano-scratch experiments of UHMWPE and N_2^+UHMWPE samples.

Values reported in Table 1 demonstrate that UHMWPE friction coefficient decreased ~30% after N_2^+ irradiation. This reduction is consistent with the increase in surface hardness and yield stress and with a reduction in the adhesion forces between the spherical indenter and the polymer due to the lower contact area during scratching (see h_{scr} values in Table 1). Additional indentation experiments performed under displacement controlled conditions (Fig. 9) showed that an inherent reduction in adhesion forces between the material surface and the indenter also occurred. In the region of negative force during unloading, the existence of adhesion forces between tip and polymers is evidenced [45]. The magnitude of adhesion forces was lower in N_2^+UHMWPE than in UHMWPE sample. This inherent reduction must be associated with changes in the chemical nature of the polymeric surface [56].

3.5. FTIR-ATR analysis

FTIR-ATR spectra of UHMWPE and N_2^+UHMWPE samples are shown in Fig. 10. Several observations can be drawn:

Spectra displayed no detectable bands in the range of 1800–1600 cm^{-1} associated with carbonyl groups [57]. As expected, post-irradiation oxidation of UHMWPE did not occur and hence the observed changes in mechanical properties are due to the effect of N_2^+ irradiation in the absence of oxygen.

N_2^+ irradiation induces a slight increase in crystalline fraction as reflected by enlargement of the intensities ratio of bands associated with crystalline and amorphous domains (1473 and 1463 cm^{-1}) [57–59]. Growth of new crystal lamellae in UHMWPE has been attributed to relaxation of local stresses as a consequence of scission of tie molecules induced by high energy radiations [57,60,61]. It is well known that UHMWPE elastic modulus scales with its crystalline fraction [5,38], so the increase in surface elastic modulus after irradiation can be related to the change in crystallinity.

UHMWPE has a simple molecular structure that contains C–H and C–C bonds. The formation of chain unsaturations (C=C bonds)

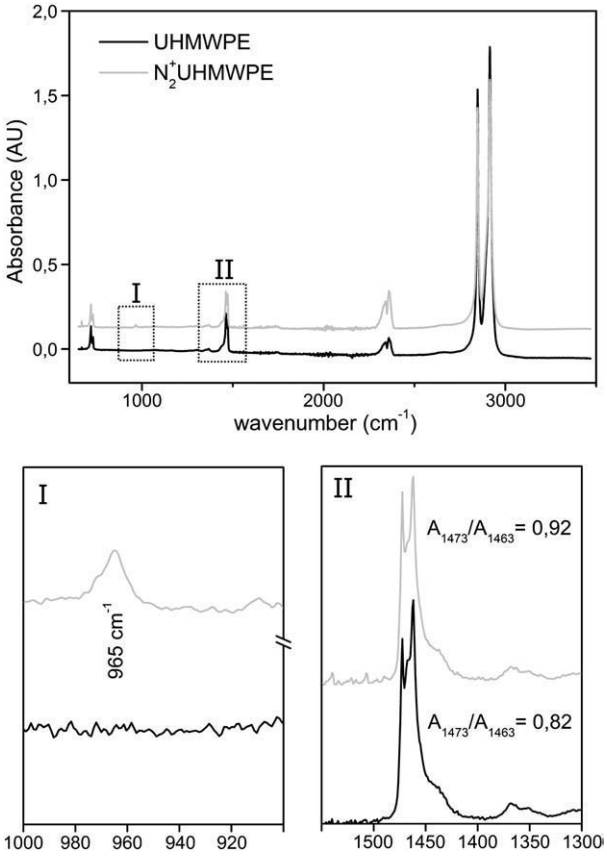

Fig. 10. FTIR-ATR spectra of UHMWPE and N_2^+UHMWPE samples. The whole range of wavenumber measured is shown on the top while the two ranges used in the analysis are amplified at bottom.

represents one of the main effects of the radiation induced chemical changes in polyethylene. Spectra of N_2^+ UHMWPE sample display a band at 965 cm^{-1} characteristic of *trans*-vinylene groups and a slight band at 910 cm^{-1} typical of vinyl groups [57,62]. A relationship between *trans*-vinylene yield and crosslinking has been established [62–64]. Highly crosslinked UHMWPE produced by γ rays or *e*-beam irradiations exhibits lower bulk and surface elastic modulus than uncrosslinked UHMWPE [7,10,31,65–67]. This is because massive crosslinking is accompanied by a reduction in crystallinity. Consequently, the increase observed in elastic modulus indicates that molecular chain crosslinking is not the main effect caused by the used N_2^+ irradiation.

N_2^+ UHMWPE spectra display no bands in the range between 1800 and 1400 cm^{-1} associated with the formation of a graphite-like structure as the one induced by ion beam implantation [11]. Such structure displays elastic modulus values closed to the ones of the pure graphite (about 4 GPa). The absence of graphitization has been previously shown [23]. It is due to the low fluence used (1×10^{12} ions/cm^2) in N_2^+ irradiation, which is three order of magnitude lesser than the fluence values used in ion beam implantation.

4. Conclusions

Surface mechanical properties and nano-tribological behavior of pristine and SHI irradiated (N_2^+ ions, energy of 33 MeV and fluence value of 1×10^{12} ions/cm^2) UHMWPE were examined by depth sensing indentation (DSI) and Scanning probe microscopy (SPM). From this investigation, the following remarks emerged:

SHI irradiation was able to greatly improve nano-wear and creep behaviour of UHMWPE.

After SHI irradiation, a modified layer of 40 μm in depth with larger elastic modulus, larger hardness, higher hardness to elastic modulus ratio and lower friction coefficient was generated.

The improvement in wear performance turned out to occur without detriment of elastic modulus and yield stress, unlike modifications induced by γ or *e* beam irradiation.

The improvement of abrasive wear resistance was related to higher material hardness and lower friction coefficient while the better adhesive wear performance was due to the lower friction coefficient together with a beneficial H/E ratio.

SHI irradiation did not promote the formation of a dehydrogenated graphite-like structure in the surface layer consistently with the low ion fluence used.

Changes in surface mechanical properties arose from the formation of carbon–carbon double bonds and the increase of crystallinity.

Further investigations regarding the effect of the swift heavy ion type and fluence on the surface mechanical response of UHMWPE are currently in progress.

Acknowledgments

This work was financially supported by the following projects: PICT-01160, PICT12-08922, PICT25530 and PIP6253. Authors would like to thank Dr. Diana Fasce for performing FTIR experiments and her valuable help in interpreting them.

References

[1] S. Li, A.H. Burstein, J. Bone Joint Surg. 76 (1994) 1080.
[2] Y.H. Zhu, K.Y. Chiu, W.M. Tang, J. Orthop. Sur. 9 (2001) 91.
[3] W. Harris, J. Biomed. Mater. Res. 31 (1996) 19.
[4] B.K. Ping Wong, S. Sinha, J.P. Ying Tan, K. Yang Zeng, Tribol. Lett. 17 (2004) 613.
[5] L.A. Pruitt, Proceedings of 13th International Meeting on the Deformation, Yield and Fracture of Polymers, Eindhoven, Netherlands, 2006.
[6] P. Bracco, V. Brunella, M.P. Luda, M. Zanetti, L. Costa, Polymer 46 (2005) 10648.
[7] L.A. Pruit, Biomaterials 26 (2005) 905.
[8] K.S. Simis, A. Bistolfi, A. Bellare, L.A. Pruitt, Biomaterials 27 (2006) 1688.
[9] A. Chapiro, Nucl. Instrum. Meth. B 105 (1995) 5.
[10] G. Lewis, Biomaterials 22 (2001) 371.
[11] A. Valenza, A.M. Visco, L. Torrisi, N. Campo, Polymer 45 (2004) 1707.
[12] D.M. Bielinski, P. Lipinski, M. Urbaniak, J. Jagielsky, Tribol. Lett. 23 (2006) 139.
[13] A. Tóth, T. Ujvári, I. Bertóri, E. Szilgágyi, T. Keszthelyi, A. Juhász, Surf. Interface Anal. 36 (2004) 1041.
[14] D.M. Bielinski, D. Tranchida, P. Lipinski, J. Jagielski, A. Turos, Vacuum 81 (2007) 1256.
[15] J.S. Chen, S.P. Lau, Z. Sun, B.K. Tay, G.Q. Yu, F.Y. Zhu, D.Z. Zhu, H.J. Xu, Surf. Coat. Technol. 138 (2001) 33.
[16] R.J. Rodríguez, A. Medrano, J.A. García, G.G. Fuentes, R. Martínez, J.A. Puertolas, Surf. Coat. Technol. 201 (2007) 8146.
[17] A. Toth, M. Mohai, T. Ujvari, I. Bertoti, Surf. Interface Anal. 38 (2006) 759.
[18] H. Dong, T. Bell, C. Blawert, B.L. Mordike, J. Mater. Sci. Lett. 19 (2000) 1147.
[19] W. Shi, X.Y. Li, H. Dong, Wear 250 (2001) 544.
[20] K.G. Kostov, M. Ueda, I.H. Tan, N.F. Leite, A.F. Beloto, G.F. Gomes, Surf. Coat. Technol. 186 (2004) 287.
[21] H. Dong, T. Bell, Surf. Coat. Technol. 111 (1999) 29.
[22] J. Jagielski, A. Piatkowska, P. Aubert, L. Thomé, A. Turos, A. Abdul Kader, Surf. Coat. Technol. 200 (2006) 6355.
[23] M.F. del Grosso, V.C. Chappa, G. García Bermúdez, E. Forlerer, M. Behar, Surf. Coat. Technol. 202 (2008) 4227.
[24] M.F. del Grosso, V.C. Chappa, G. García Bermúdez, AIP Conference Proceedings 947 (2007) 473.
[25] V.C. Chappa, M.F. del Grosso, G. García Bermúdez, R.O. Mazzei, Nucl. Instrum. Meth. B 243 (2006) 58.
[26] E. Balanzat, N. Betz, S. Bouffard, Nucl. Instrum. Meth. B 105 (1995) 46.
[27] V. Picq, J.M. Ramillon, E. Balanzat, Nucl. Instrum. Meth. B 146 (1998) 496.
[28] L. Singh, R. Singh, Nucl. Instrum. Meth. B 225 (2004) 478.
[29] M. Melot, Y. Ngono-Ravache, E. Balanzat, Nucl. Instrum. Meth. B 209 (2003) 205.
[30] M.F. del Grosso, V.C. Chappa, G. García Bermudez, R.O. Mazzei, Nucl. Instrum. Meth. B 245 (2006) 281.
[31] J. Zhou, A. Chakravartula, L. Pruitt, K. Komvopoulos, Trans. ASME 126 (2004) 386.
[32] B.K. Ping Wong, S.K. Sinha, J.P. Ying Tan, K.Y. Zeng, Tribol. Lett. 17 (2004) 613.
[33] C. Charitidis, S. Logothetidis, Comp. Mater. Sci. 33 (2005) 296.
[34] S.P. Ho, L. Riester, M. Drews, T. Boland, M. LaBerge, Instrum. Mech. Eng. H 217 (2003) 357.
[35] K.B. Geng, F.Q. Yang, T. Druffel, E.A. Grulke, Polymer 46 (2005) 11768.
[36] B.J. Briscoe, L. Fiori, E. Pelillo, J. Phys, D: Appl. Phys. 31 (1998) 2395.
[37] M. Nowicki, A. Richter, B. Wolf, H. Kaczmar, Polymer 44 (2003) 6599.
[38] K. Park, S. Mishra, G. Lewis, J. Losby, Z. Fan, J.B. Park, Biomaterials 25 (2004) 2427.
[39] J.E. Ziegler, J.P. Biersack, U. Littmark, Pergamon, New York, 1985.

[40] J. Cayer-Barrioz, D. Mazuyer, A. Tonck, P. Kapsa, A. Chateauminois, Tribol. Int. 39 (2006) 62.
[41] W.C. Oliver, G.M. Pharr, J. Mater. Res. 7 (1992) 1562.
[42] B. Beake, J. Phys, D. Appl. Phys. 39 (2006) 4478.
[43] N.K. Myshkin, M.I. Petrokevets, A.V. Kovalev, Tribol. Int. 38 (2005) 910.
[44] International standard ISO 14577-1 (2002) Metallic materials — Instrumented indentation test for hardness and materials parameters.
[45] D.M. Ebenstein, L.A. Pruitt, Nanotoday 1 (2006) 26.
[46] K.B. Geng, F.Q. Yang, T. Druffel, E.A. Grulke, Polymer 46 (2005) 11768.
[47] A.H.W. Ngan, B. Tang, J. Mater. Res. 17 (2002) 2604.
[48] A.H.W. Ngan, H.T. Wang, B. Tang, K.Y. Sze, Int. J. Solids Struct. 42 (2005) 1831.
[49] B. Tang, A.H.W. Ngan, J. Mater. Res. 18 (2003) 1141.
[50] P. Berke, F. El Houdaigui, T.J. Massart, Wear 268 (2010) 223.
[51] A.C. Fisher-Cripps, Surf. Coat. Technol. 168 (2003) 136.
[52] A.C. Fischer-Cripps, 2nd Ed.Springer, New York, 2007.
[53] A. Flores, F.J. Baltá Calleja, G.E. Attenburrow, D.C. Bassett, Polymer 41 (2000) 5431.
[54] S.N. Ratner, I.I. Farberoua, O.V. Radyukeuich, E.G. Lure, Sovietic Plastics 7 (1964) 37.
[55] E. Rabinowicz, J. Wiley & Sons. Ltd., New York, 1965.
[56] D. Tabor, Advances in polymer friction and wear, in: Lee (Ed.), Polym. Sci. Technol., 207, 1974, pp. 3887–3894.
[57] O.N. Trtinnikov, S.-I. Fujita, S. Ogata, Y. Ikada, J. Polym. Sci., Part B: Polym. Phys. 37 (1999) 1503.
[58] G. Zerby, G. Gallino, N.D. Fanty, L. Baini, Polymer 30 (1989) 2324.
[59] H. Hagemann, R.G. Snyder, A.J. Peacock, J. Mandelkern, Macromolecules 22 (1989) 3600.
[60] A. Shinde, R. Salovey, J. Polym. Sci. Polym. Phys. 23 (1985) 1681.
[61] S.K. Bhateja, E.H. Andrews, R.J. Young, Polym. Sci. Polym. Phys. 21 (1983) 523.
[62] P. Bracco, V. Brunella, M.P. Luda, M. Zanetti, L. Costa, Polymer 46 (2008) 10648.
[63] O.K. Muratoglu, W.H. Harris, J. Biomed. Mater. Res. 56 (2001) 584.
[64] W.C. Johnson, B.J. Lyons, Rad. Phys. Chem. 46 (1995) 829.
[65] H.A. Khonakdar, J. Morshedian, U. Wagebknecht, S.H. Jafari, Polymer 44 (2003) 4301.
[66] J.L. Gilbert, J. Cumber, A. Butterfield, J. Biomed. Mater. Res. 61 (2002) 270.
[67] M. Roy, Mat. Res. Soc Symp Proc. 847 (2005) 1541.